Chemical Engineering Journal 161 (2010) 301–307

Contents lists available at ScienceDirect

Chemical Engineering Journal

journal homepage: www.elsevier.com/locate/cej

Preparation and characterization of attapulgite/polyaniline nanofibers via self-assembling and graft polymerization

Liang Shao [a], Jianhui Qiu [a,b,*], Mingzhu Liu [a,**], Huixia Feng [c], Guohong Zhang [b], Shaoyu Lü [a], Lijun Qin [a]

[a] College of Chemistry and Chemical Engineering, Lanzhou University, Lanzhou 730000, PR China
[b] Department of Machine Intelligence and Systems Engineering, Faculty of Systems Engineering, Akita Prefectural University, Akita 015-0055, Japan
[c] College of Petrochemical Technology, Lanzhou University of Technology, Lanzhou 730050, PR China

ARTICLE INFO

Article history:
Received 5 December 2009
Received in revised form 13 April 2010
Accepted 16 April 2010

Keywords:
Attapulgite
Polyaniline
Nanofibers
Conductivity
Stability

ABSTRACT

Core–shell conducting nanofibers SAM-ATP/PANI were prepared by the encapsulation of attapulgite (ATP) template with polyaniline (PANI) after the surface modification with γ-aminopropyltriethoxysilane (APTES) to form a self-assembled monolayer (SAM) on the surface of ATP needle-shaped particle (SAM-ATP). The conductivity of 18.7 wt% SAM-ATP/PANI nanofibers at room temperature was determined to be (2.21 ± 0.17 S/cm), larger than pure PANI (0.47 ± 0.02 S/cm). Moreover, the conductivity stability and thermal stability of 18.7 wt% SAM-ATP/PANI nanofibers were clearly improved. These trends were accompanied by significant structural changes as evidenced by Transmission electron microscopy, Fourier transform IR, X-ray diffraction analysis and UV–visible spectroscopy.

1. Introduction

The discovery of conducting polymers and their doping over the full range from insulator to metal by Heeger, MacDiarmid, Shirakawa and co-workers has been landmark research leading to what has been designated as the "fourth generation of polymer materials". Polyaniline (PANI) is a representative of the electroactive synthetic material family [1,2]. The promise of polymer electronics depends in part on the development of stable conductive materials that can be inexpensively processed [3,4]. Therefore stability is an extremely important factor especially for materials applied under harsh circumstances. Additionally, other shortcomings of PANI are its limited room temperature conductivity and high temperature dependence of conductivity, which the conductivities at room and high temperature are important properties for conducting polymers in most commercial applications such as conducting coatings, electronic circuits, and polymer electrolyte membranes for fuel cells [5–8].

Attapulgite (or palygorskite-as it often called) (ATP) is a crystalline hydrated magnesium aluminum silicate with unique three-dimensional structure and has a fibrous morphology. Attapulgite has the structural formula $Si_8O_{20}Mg_5(Al)(OH)_2(H_2O)_4{\cdot}4H_2O$, and its ideal structure is studied by Moolchandra early in 1972 [9]. There have been some reports of the use of ATP in rubbers, adhesives, thermoplastic polymers, silicate/epoxy nanocomposite, catalyst supports and environmental absorbents [10–14].

In this paper, we prepared the ATP/PANI nanofibers with well-covered core–shell morphology for the first time. We selected ATP as the host because of its important advantage: (a) ATP is a type of natural fibrillar silicate clay mineral, and its fibrillar single crystal is the smallest structure unit with a length of ~500 and ~20 nm in diameter; (b) it is an inactive inorganic host without redox character, so the polymerization can be controlled; (c) it has a large surface area and stronger absorptive capacity than any other natural minerals. The aim of this work was to prepare the core–shell conducting nanofibers by the encapsulation of ATP template with PANI via graft polymerization after the surface modification with γ-aminopropyltriethoxysilane (APTES) to form a self-assembled monolayer (SAM) on the surface of ATP needle-shaped particle (SAM-ATP).

Along with being characterized, the conductivities of SAM-ATP/PANI nanocomposites are higher in comparison with other PANI–clay composites that have been reported [11,14,15]. Moreover, the experiments reveal that the presence of SAM-ATP improved the conductivity stability, thermal stability and dispersion effect of SAM-ATP/PANI nanofibers. Samples of SAM-ATP/PANI nanofibers were characterized by Fourier transform IR (FTIR) spectroscopy, X-ray diffraction analysis (XRD), UV–visible spectroscopy, thermogravimetric analysis (TGA) and conductivity measurements. Transmission electron microscopy (TEM) was used to study the morphologies of the SAM-ATP/PANI nanofibers.

* Corresponding author. Tel.: +81 184 27 2134; fax: +81 184 27 2188.
** Corresponding author. Tel.: +86 931 8912387; fax: +86 931 8912582.
E-mail addresses: qiu@akita-pu.ac.jp (J. Qiu), m-zliu@163.com (M. Liu).

1385-8947/$ – see front matter © 2010 Elsevier B.V. All rights reserved.
doi:10.1016/j.cej.2010.04.033

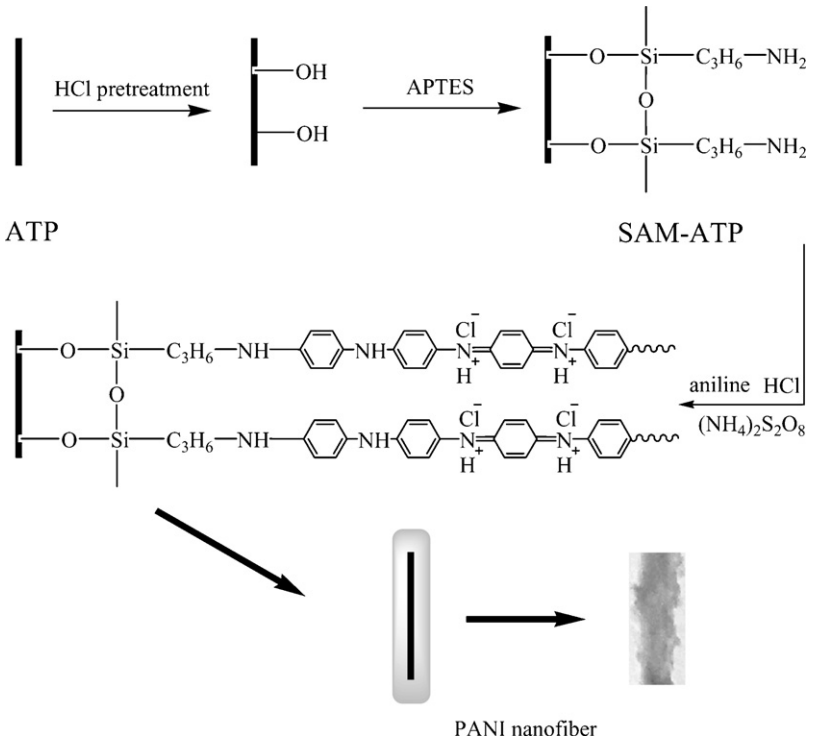

Fig. 1. Preparation routes of SAM-ATP/PANI nanofibers.

2. Experimental

2.1. Materials

Attapulgite (ATP) nano-fibrillar clay with average diameter of 20 nm was provided by Toshin Chemicals Limited Company, Japan. Aniline monomer (purity 99.5%, Tianjin Baishi Chemical Industry Co. Ltd., Tianjin, China) was vacuum distilled prior to use. γ-Aminopropyltriethoxysilane (APTES) was obtained from Nanjing Aocheng Chemical Co. Ltd., Nanjing, China. Toluene, ammonium persulfate (APS), hydrochloric acid (HCl), sodium bicarbonate and absolute ethanol were purchased from Tianjin Chemical Co., Tianjin, China. All chemicals were of analytical grade and used without further purification.

2.2. Preparation of SAM-ATP/PANI nanofibers

Our approach to prepare SAM-ATP/PANI nanofibers consisted of two major steps [16–18], as shown in Fig. 1. The first step was to prepare SAM-coated ATP particles (SAM-ATP), and the second step was to obtain SAM-ATP/PANI nanofibers by grafting PANI onto the SAM-ATP particles. In the first step, 45 g of ATP particles were first dispersed into 450 ml of 1 mol L^{-1} HCl aqueous solution, and the mixture was stirred for 8.5 h at 80 °C to generate a particle surface with high coverage of Si–OH groups. The particles were collected on a filtration funnel, washed repeatedly with $NaHCO_3$ aqueous solution and distilled water until neutral, and then dried at 80 °C in vacuum. Then, the particles were dispersed into a solution of APTES in toluene (1.05 mol L^{-1}) with stirring for 11 h at 110 °C, and then the unreacted APTES was extracted with absolute ethanol in a Soxhlet apparatus. The SAM-ATP particles were finally dried.

In the second step, 1 ml of distilled aniline was added to 89 ml of 1 mol L^{-1} HCl aqueous solution, and then SAM-ATP particles (0.03–1.50 g) were dispersed in the reaction mixture under a nitrogen atmosphere with ultrasonic vibrations for 15 min. After that, 10 ml of APS solution (0.11 mol L^{-1} in the reaction system) was given dropwise within 15 min under stirring in the solution to start the polymerization, and the mixture was allowed to polymerize under a nitrogen atmosphere for another 9 h at 0–5 °C. Then SAM-ATP/PANI nanocomposites were collected on a filtration funnel, washed repeatedly with distilled water until the filtrate was neutral to ensure that the excess of acid was removed, followed by washing with ethanol several times. At last SAM-ATP/PANI nanocomposites were obtained after dried at 25 °C in vacuum. The prepared SAM-ATP/PANI nanocomposites contained 4.6–76.7 wt% of SAM-ATP (0.03–1.50 g) in SAM-ATP/PANI nanocomposites by weight.

2.3. Preparation of neat-ATP/PANI composites

As a control, neat-ATP/PANI composites particles were also prepared by using chemical oxidative polymerization of aniline in the presence of neat-ATP particles without HCl pretreatment and SAM coating. The resultant composite particles were referred to as neat-ATP/PANI. The prepared ATP/PANI nanocomposites contained 4.7–48.8 wt% of ATP (0.03–0.50 g) in neat-ATP/PANI nanocomposites by weight.

2.4. Characterization techniques

The electrical conductivities of the PANI nanocomposite powders were measured using a four-probe device (KDY-1 Resistivity Measuring Instrument, Kunde Technology Co. Ltd., Guangzhou, China) at ambient temperature employing the method on a pressed pellet according to the formula:

$$\sigma = \left(\frac{1}{\rho}\right) = \left(\frac{V}{I}\right) \times F\left(\frac{D}{S}\right) \times F\left(\frac{W}{S}\right) W \times F_{sp}$$

where σ referred to electrical conductivity, V the voltage, I the current, D the diameter of the pallets, W the thickness of the pallets,

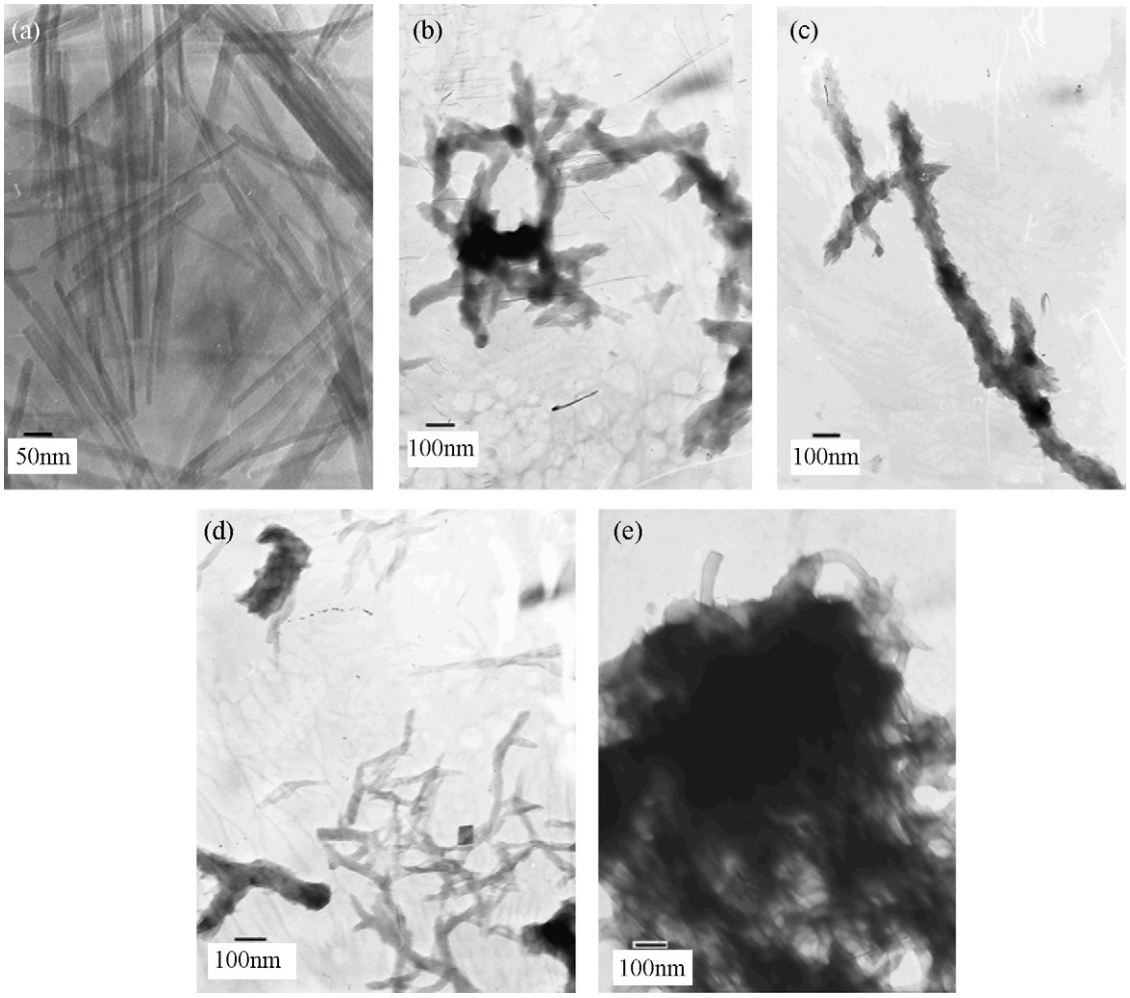

Fig. 2. The TEM images: (a) neat-ATP; (b) 4.6 wt% SAM-ATP/PANI; (c) 18.7 wt% SAM-ATP/PANI; (d) 32.6 wt% SAM-ATP/PANI and (e) 20.1 wt% neat-ATP/PANI.

S the average space between the probes, $F(D/S)$ the amendatory coefficient of the diameter of the pallets, $F(W/S)$ the amendatory coefficient of the thickness of the pallets and F_{sp} was the amendatory coefficient of the space between the probes. The pellets with 13 mm diameter and about 1.5 mm thickness were obtained by subjecting the powder samples to a pressure of 8 ton. For the decreasing of the measurement errors, the reproducibility of the result was checked by measuring the electrical conductivity three times for each pellet, and the average value was used. The temperature dependence of conductivity was determined by WDJ-1 Temperature Change Resistance Measuring Instrument (Institute of Chemistry the Chinese Academy of Sciences) at a heating rate of 10 °C/min from 25 to 155 °C.

FTIR measurements (Impact 400, Nicolet, Waltham, MA) were carried out with the KBr pellet method. Electronic absorption spectra of SAM-ATP/PANI and PANI were recorded in DMF solvent in the wavelength range of 290–850 nm at room temperature using the Lamda 35 UV–visible spectrophotometer (PerkinElmer, USA). TA Instrument 2050 thermogravimetric analyzer was used for TGA; heating rate was 10 °C/min from 25 to 550 °C in the air. X-ray diffraction (XRD) patterns were recorded in the range of $2\theta = 2–50°$ by step scanning with XRD-6000 (Shimadzu, Japan). Nickel-filter Cu Kα radiation ($\lambda = 0.15418$ nm) was used with a generator voltage of 40 kV and a current of 30 mA. Elemental analysis of C, N, and H was performed on Elementar vario EL instrument. The morphologies of the nanofibers were characterized with a JEM-1200 EX/S transmission electron microscope (TEM) (JEOL, Tokyo, Japan).

3. Results and discussion

3.1. Microstructure characterization

Neat-ATP is a type of natural fibrillar silicate clay mineral with a length of ~500 and ~20 nm in diameter as shown in Fig. 2a. Fig. 2b–d shows the SAM-ATP/PANI nanofibers synthesized with different amounts of SAM-ATP vary greatly and the diameter/length ratio of SAM-ATP/PANI nanofibers is about 1/7.5. It is obvious that SAM-ATP/PANI nanofibers (Fig. 2b and c) give well-covered core–shell structure, and their diameters increase from about 20 nm of the neat-ATP (Fig. 2a) to about 70 nm. However, the core–shell structure is not obvious with excess SAM-ATP was added as shown in Fig. 2d.

From Fig. 2c, the surface of needle-shaped particles are covered with compact and transparent shagginess and the PANI coating of SAM-ATP needle-shaped particles are complete and well-dispersed [14,16,18]. Moreover, the best coating effect unfold a crystalline order and kept connective with PANI chains, which could be the most likely reason for the influence on the room temperature conductivity and temperature dependence of conductivity correspondingly [19,20].

Fig. 2c and e shows the surface images of 18.7 wt% SAM-ATP/PANI nanofibers and 20.1 wt% neat-ATP/PANI. Compare with well-covered core–shell structure of 18.7 wt% SAM-ATP/PANI nanofibers (Fig. 2c), amorphous PANI do not well disperse and aggregate significantly in the surface of neat-ATP by physical

Table 1
Results of elemental analysis for ATP.

	Element analysis (wt%)		
	N	C	H
Neat-ATP	0.000	0.722	1.253
SAM-ATP	1.451	4.638	1.563

adsorption (Fig. 2e). On one hand, it is obvious that SAM-ATP needle-shaped particles show better dispersion because of the effect of hydrophobic alkyl group of the modified agent APTES [14]. On the other hand, in the preparation approach, APTES was selected as a coupling agent, which had two functions from its functional groups. That was, a dense SAM was formed when it reacted with –OH groups on the surface of HCl-treated ATP nanoparticles in the first step. Because the attached silane chains possessed a reactive end $–NH_2$ group, PANI chains could be grafted chemically on ATP easily in the second step. The possible polymerization mechanism is illustrated in Fig. 1, similar to the mechanism that was proposed by Sutar [16] and Jing [18], respectively.

3.2. Elemental analysis

The untreated APTES is completely removed with absolute ethanol in the Soxhlet apparatus. As confirmed by the elemental analysis results in Table 1, the SAM-ATP shows the higher relative contents of nitrogen and carbon with respect to neat-ATP which is indicative of the participation of APTES to form a SAM on the surface of ATP needle-shaped particles. In this preparation approach, APTES is selected as a coupling agent and SAM is formed when it reacts with –OH groups on the surface of HCl-treated ATP needle-shaped particles [18].

3.3. Conductivity characteristics

The effects of the ATP (SAM-ATP and neat-ATP) weight percent on the conductivity of the resulting nanocomposites are presented in Fig. 3a and b.

As we can see from Fig. 3a, with SAM-ATP weight fraction increasing, the conductivities have been obviously enhanced in the earlier phase and weakened later. That is to say, there is a maximum conductivity of 2.21 ± 0.17 S/cm at 18.7 wt% SAM-ATP/PANI which give well-covered core–shell structure nanofibers because of APTES as a coupling agent as shown in Fig. 2c. It is considered that SAM-ATP is helpful to form this structure, which is conducive to better conductivity at the origin of the high electric conductivity observe. On one hand, SAM-ATP as a template takes a conformation

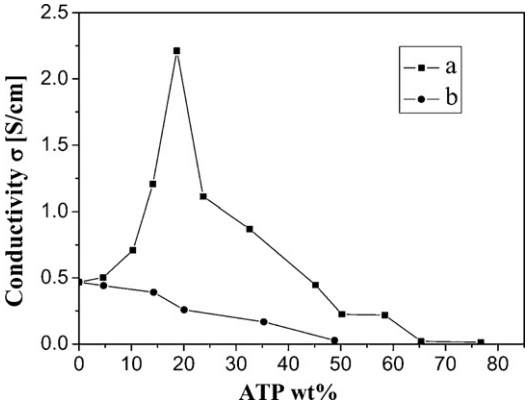

Fig. 3. Effect of ATP (SAM-ATP and neat-ATP) weight fractions on the conductivity of nanocomposites: (a) SAM-ATP/PANI and (b) neat-ATP/PANI.

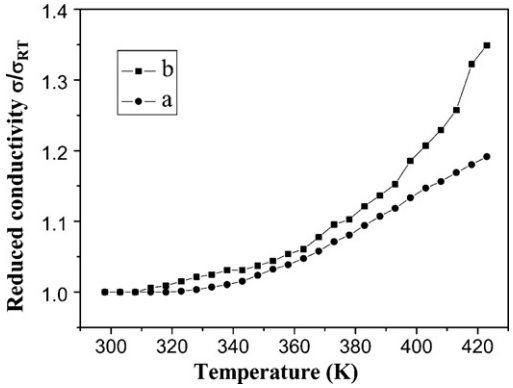

Fig. 4. Temperature dependence of conductivity of 18.7 wt% SAM-ATP/PANI and 20.1 wt% neat-ATP/PANI: (a) 18.7 wt% SAM-ATP/PANI and (b) 20.1 wt% neat-ATP/PANI.

with more extended chains than pure PANI, leading to a greater conjugation, and this would make the transition easier because of a lower energy gap. As a result, the conductivities have been increased. Moreover, this could be proved by UV–visible spectra. Additionally, it is believed that the extended chain conformation could result in the complex aggregate growing as fibers [15,21–26]. In our system, the similar fibers (diameter about 70 nm) are also observed as shown in Fig. 2c, which further proves the formation of the extended chains. On the other hand, this extended chain conformation would unfold with a crystalline order and would improve the alignment of the PANI chains in the amorphous conductive grains increasing their conductivity [15,26–28]. However, the conductivities of SAM-ATP/PANI decrease with the excess of SAM-ATP. The possible explanation is that the SAM-ATP component are not conductive and only the PANI component contribute to the observe conductivity. Moreover, the incorporation of SAM-ATP results in a significant increase in isolated molecular PANI chains in the SAM-ATP/PANI composites leading to an observable reduction of conductivity [29,30].

As shown in Fig. 3a and b, the conductivities of SAM-ATP/PANI are obviously improved compared with neat-ATP/PANI. It is speculated that PANI, which is aggregate in the surface of neat-ATP (as shown in Fig. 2e) by physical adsorption effect, could not improve the crystalline order. Moreover, as mentioned above, ATP component was not conductive and only the PANI component contributed to the observed conductivity. Therefore, the conductivities of neat-ATP/PANI decreased compared with pure PANI (0.47 S/cm).

3.4. Temperature dependence of conductivity

Fig. 4 shows the variation of the conductivity of the 18.7 wt% SAM-ATP/PANI and 20.1 wt% neat-ATP/PANI pellets upon heating from 298 to 425 K in air. As the *Y*-axis, we have chosen σ/σ_{RT} (RT = room temperature) rather than the absolute value of the conductivity (σ) because this presentation allows for a better comparison of temperature dependence of conductivity since all curves start from the same point [31].

As shown in Fig. 4, with the increasing of temperature from 298 to 425 K, the conductivity increases. This figure clearly indicates that all the samples had a semiconducting property. For semiconductors, the higher the temperature is, the higher the electrical conductivity [32]. As shown in Fig. 4, the maximum values of observed conductivities were 19% (Fig. 4a) and 35% (Fig. 4b) higher than conductivities measured in room temperature. Therefore, the 20.1 wt% neat-ATP/PANI nanocomposite has a strongly temperature dependent conductivity over the entire temperature range from 283 to 423 K. It is worth to notice that 18.7 wt% SAM-ATP/PANI nanocomposite has a weakly temperature dependent conductiv-

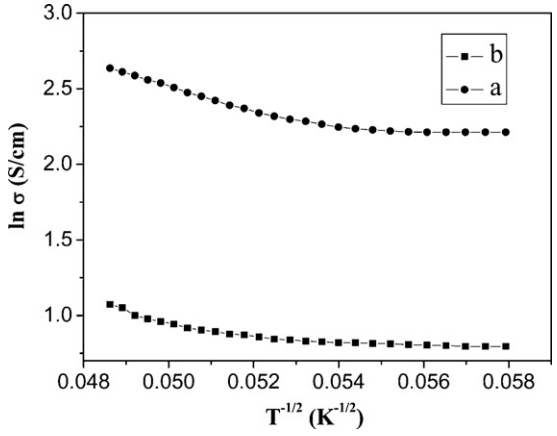

Fig. 5. Electrical conductivity σ of 18.7 wt% SAM-ATP/PANI and 20.1 wt% neat-ATP/PANI as function of temperature (T), which is expressed in relation to VRH model: (a) 18.7 wt% SAM-ATP/PANI and (b) 20.1 wt% neat-ATP/PANI.

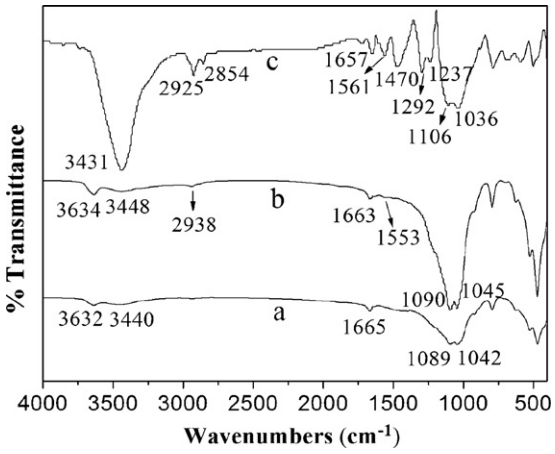

Fig. 6. FTIR spectra: (a) neat-ATP; (b) SAM-ATP and (c) 18.7 wt% SAM-ATP/PANI.

ity. However, the conductivity stabilizing effect of the polymers becomes even more obvious in the 18.7 wt% SAM-ATP/PANI. This is because PANI chains could be grafted chemically on SAM-ATP due to the presence of APTES coupling agents. It had two functions from its functional groups which were applied to promote adhesions between the PANI and the ATP. Therefore, the SAM-ATP, incorporated as parts of the complex, were strongly attached to the PANI chains, and the conductive state was found to be stable under heat. Additionally, the fact that crystalline 18.7 wt% SAM-ATP/PANI have a more fibrillar morphology might again be responsible for the better thermal stability of electrical properties [18,25,26,30].

The conduction mechanisms for conducting polymers have been investigated from various model related to temperature dependence of conductivity. Moreover, the temperature dependence of the conductivity of 18.7 wt% SAM-ATP/PANI and 20.1 wt% neat-ATP/PANI exhibited a typical semiconductor behavior that could be expressed according to variable-range hopping (VRH) model proposed by Mott [33] as follows:

$$\sigma(T) = \sigma_0 \exp\left[-\left(\frac{T_0}{T}\right)^{\gamma}\right]$$

where σ_0 is the high temperature limit of conductivity and T_0 is Mott's characteristic temperature associated with the required energies of charge carriers. It indicates a granular metal type structure, in which electrical conductivity takes place by charge carrier tunneling through insulating barriers between conductive grains [27]. The exponent $\gamma = 1/(1+d)$ determines the dimensionality of the conducting medium. The possible values of γ is 1/4, 1/3 and 1/2 for three-, two- and one-dimensional systems, respectively. The best-fitted value of γ is obtained by the linear regression analysis. The lowest standard deviations are found for $\gamma = 1/2$ for 18.7 wt% SAM-ATP/PANI and 20.1 wt% neat-ATP/PANI respectively. By plotting $\ln(\sigma)$ vs $T^{-1/2}$, the linear dependence of $\ln(\sigma)$ on $T^{-1/2}$ are shown in Fig. 5, indicating that one-dimensional (1D) charge transport occurs in the ATP/PANI composites. The T_0 value could be obtained from the slope of Fig. 5 and are given in Table 2. The T_0 value of 18.7 wt% SAM-ATP/PANI nanofibers (407 K) is lower than that of 20.1 wt% neat-ATP/PANI (836 K), which is consistent with the results obtained from room temperature conductivity measurements [34–36].

In addition, the activation energy of conduction can be evaluated by an Arrhenius equation described as follows:

$$\sigma_{dc} = \sigma_0 \exp\left(\frac{-E_a}{KT}\right)$$

where σ_{dc} denotes the electrical conductivity; σ_0 is the pre-exponential factor which can be obtained from the intercepts of the straight line (Fig. 5 and Table 2); K is the Boltzmann constant ($K = 1.38 \times 10^{-23}$ J/K); T represents the absolute temperature and E_a is the activation energy of conduction. As for Arrhenius equation, the relationship between the conducting behavior and activation energy could be described. In other words, the lower activation energy of conduction, which is evaluated by an Arrhenius equation, is also evidence of the highly conducting behavior of the composites. E_a could be calculated at room temperature and are given in Table 2. As shown in Table 2, the E_a of 18.7 wt% SAM-ATP/PANI nanofibers (0.029 eV) is lower than that of 20.1 wt% neat-ATP/PANI nanocomposites (0.041 eV) at room temperature. Therefore, this could be seen as a theoretic reason of the highly conducting behavior of the present 18.7 wt% SAM-ATP/PANI nanofibers [37,38].

Table 2
T_0, σ_0 and E_a as defined by VRH model and Arrhenius equation.

Samples	T_0 (K)	σ_0 (S/cm)	E_a (eV)
20.1 wt% neat-ATP/PANI	836	4.02	0.041
18.7 wt% SAM-ATP/PANI	407	6.83	0.029

3.5. FTIR spectra analysis

In the preparation of SAM-ATP/PANI nanofibers, the SAM coating is a very important step. Chemical anchoring of a SAM onto ATP surface have been confirmed by FTIR measurements. Fig. 6a and b represent the FTIR absorption spectra of neat-ATP and SAM-ATP. It is noticed that, the new peak at 2938 cm^{-1} is appear in Fig. 6b but not appear in Fig. 6a, and this peak is assigned to the stretching vibrations of $-CH_2$ in the SAM-ATP, indicating that the formation of a well-defined SAM layer. The new band at 1553 cm^{-1} is assigned to the stretching vibrations of N–H appeared in the spectrum of the SAM-PANI (Fig. 6b), providing further evidence for this attachment [14,18].

The FTIR characteristic peaks of 18.7 wt% SAM-ATP/PANI nanofibers are shown in Fig. 6c. The main peaks consistent with quinone and benzene ring can be observed at 1561 and 1470 cm^{-1}. The absorption band at 1292 cm^{-1} is C–N stretching of secondary aromatic amine. The band characteristic of the conducting protonated form is observed at about 1237 cm^{-1} and interpreted as a $C–N^{\bullet+}$ stretching vibration in the polaron structure [39–41]. The characteristic peaks of SAM-ATP are at 3431, 2923, 1657, 1561, 1106 and 1036 cm^{-1} as shown in 18.7 wt% SAM-ATP/PANI nanofibers [11,14,42].

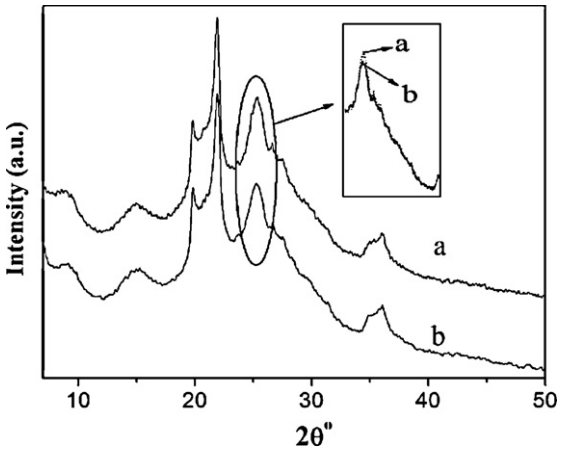

Fig. 7. XRD patterns: (a) 18.7 wt% SAM-ATP/PANI and (b) 20.1 wt% neat-ATP/PANI.

3.6. XRD analysis

Fig. 7 shows there is a distinct peak at $2\theta = 25^\circ$ (intensity = 4415 a.u.) in 18.7 wt% SAM-ATP/PANI nanofibers, which is more intenser than the corresponding peak in the X-ray pattern of 20.1 wt% neat-ATP/PANI (intensity = 4188 a.u.). According to the reports of Bruno [31] and Jan [25], PANI denoted as "amorphous", contained a marginal fraction of a crystalline phase, characterized by the broad faint reflection at $2\theta = 25^\circ$ which corresponds to the periodicity in the chain-ion-chain stacking direction and is indexed as 0 4 0 in the monoclinic cell. The above observation suggests more ordered stacking and a larger coherence length in the chain stacking direction in PANI by the encapsulation of SAM-ATP template via graft polymerization. In addition to this remarkably intense and narrower reflection at $2\theta = 25^\circ$, the shift from $2\theta = 8.64^\circ$ (d-spacing = 1.022 nm) to 9.01° (d-spacing = 0.980 nm) in the lower angle region indicated that 18.7 wt% SAM-ATP/PANI nanofibers increased the inter-planar distance and crystallinity ordered correspondingly [43–45].

Therefore, according to the XRD analysis shown in Fig. 7, there were some evidences obtained for the illustration about conductivity characteristics and temperature dependence of conductivity we made above.

3.7. UV-visible spectroscopy

The UV–visible spectra of pure PANI and SAM-ATP/PANI nanocomposites are shown in Fig. 8. The characteristic bands of the PANI at about 310 and 550 nm are clearly observed. These bands are attributed to the $\pi \rightarrow \pi^*$ and $n \rightarrow \pi^*$ transitions, which can be related to the degree of conjugation along the main chain [29,46].

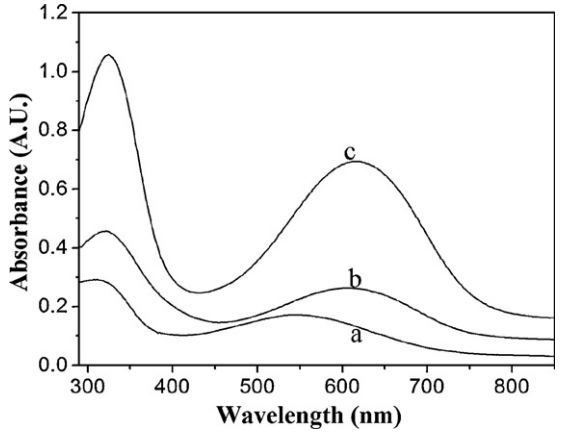

Fig. 8. UV–visible spectra of pure PANI and SAM-ATP/PANI nanocomposites: (a) pure PANI; (b) 14.1 wt% SAM-ATP/PANI and (c) 18.7 wt% SAM-ATP/PANI.

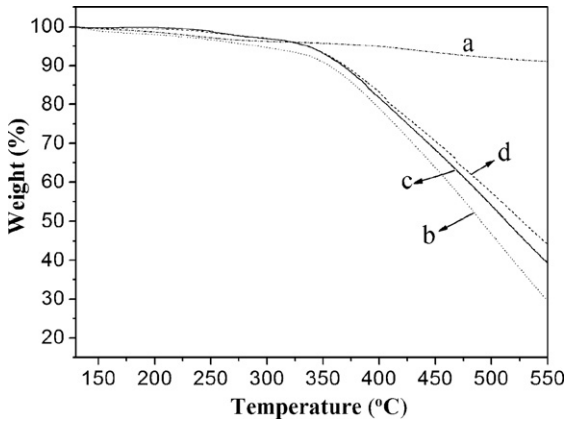

Fig. 9. TGA thermograms: (a) neat-ATP; (b) pure PANI; (c) 20.1 wt% neat-ATP/PANI and (d) 18.7 wt% SAM-ATP/PANI.

By comparing the curves a–c in Fig. 8, it shows that the peaks for the $\pi \rightarrow \pi^*$ and $n \rightarrow \pi^*$ transitions were red shifted as the content of SAM-ATP increased. The red shift would suggest a greater conjugation and this would make the transition easier because of a lower energy gap. As a result, the conductivities have been increased [46,47]. This coincides with the high conducting behavior of 18.7 wt% SAM-ATP/PANI nanocomposites.

3.8. Thermal stability

According to the TGA curves shown in Fig. 9, the first stage below 130 °C is mainly due to the removal of free water. As the X-axis, we have started from 130 °C rather than room temperature because this presentation allows for a better comparison of thermal stability. The thermal degradation of the PANI occurs at ~200 °C which is mainly due to dopant anions from the PANI. A sharp loss in mass is observed at 320 °C, possibly due to a large-scale thermal degradation of the PANI chains [18].

According to previous work, the thermal stability of polymer filled with ATP was improved to some extent [14,48]. In this study, it can also be observed that the thermal stability of ATP/PANI increases by about 40 °C (200 → 240 °C) comparing with pure PANI. Additionally, comparing with these curves, the weight loss at 550 °C in pure PANI (72.3%) is much more than that in ATP/PANI nanocomposites, which could be attributed to the ATP silicate acting as heat resistance material [12,14].

With a comparison of TGA curves of 18.7 wt% SAM-ATP/PANI nanofibers and 20.1 wt% neat-ATP/PANI nanocomposites, it is known that both composites yield similar thermal degradation behaviors at temperatures lower than 320 °C. However, the degradation of the polymer is markedly depresses at temperatures from 320 to 550 °C, being reflected by the lower degradation rate (curve d). ATP silicate with excellent thermal stability below 550 °C (as shown in Fig. 9a) could be attributed as heat resistance material. However, the higher degradation of rate is observed by comparing the curves c and d in Fig. 9, though the amount of ATP in 20.1 wt% neat-ATP/PANI nanocomposites is more than that in 18.7 wt% SAM-ATP/PANI. Therefore we believe that the lower degradation of rate (Fig. 9d) is mainly attributed to the direct chemical bonding of PANI chains onto ATP surface via self-assembling and graft polymerization with coupling agent. Therefore, the 18.7 wt% SAM-ATP/PANI nanofibers have improved thermal stability over the 20.1 wt% neat-ATP/PANI composites. This increased thermal stability of 18.7 wt% SAM-ATP/PANI is possibly

attributed to the covalent bonding via PANI-grafting onto the ATP surface.

In addition, thermal stability is an extremely important factor especially for materials applied under harsh circumstances. Moreover, SAM-ATP/PANI nanofibers with high thermal stability and conductivity blends with common polymers seem to have great promise for many applications as construction material including as printer rollers, conducting glues and paint coatings for anticorrosion protection. In addition, this high thermal stability is very important when process with common polymers [49].

4. Conclusions

In summary, we prepared the core–shell conducting nanofibers by the encapsulation of attapulgite (ATP) template with PANI via graft polymerization after the surface modification with APTES to form a SAM on the surface of ATP needle-shaped particle (SAM-ATP). The room temperature conductivity of 18.7 wt% SAM-ATP/PANI nanofibers (2.21 ± 0.17 S/cm) was increased compared with pure PANI (0.47 S/cm). The conductivity stability and thermal stability of 18.7 wt% SAM-ATP/PANI nanofibers were clearly improved.

References

[1] C.K. Chiang, C.R. Fincher, Y.W. Park, A.J. Heeger, H. Shirakawa, E.J. Louis, et al., Electrical conductivity in doped polyacetylene, Phys. Rev. Lett. 39 (1977) 1098–1101.
[2] V.A. Adrian, A.S. Jose, E. Gustavo, Doping of polyaniline by acid–base chemistry: density functional calculations with periodic boundary conditions, J. Am. Chem. Soc. 127 (2005) 11318–11327.
[3] J.E. Yoo, J.L. Cross, T.L. Bucholz, Improving the electrical conductivity of polymer acid-doped polyaniline by controlling the template molecular weight, J. Mater. Chem. 7 (2007) 1268–1275.
[4] L. Marc, Chemistry: pampered by PAAMPSA, Science 316 (2007) 341–343.
[5] Y. Insun, A.D. Bhavana, L.R. Carmen, Thermal stability of high molecular weight self-doped poly(anilineboronic acid), Macromolecules 38 (2005) 10022–10026.
[6] J.X. Huang, B.K. Richard, A general chemical route to polyaniline nanofibers, J. Am. Chem. Soc. 126 (2004) 851–855.
[7] A.D. Bhavana, Y. Insun, S.F. Michael, A switchable self-doped polyaniline: interconversion between self-doped and non-self-doped forms, J. Am. Chem. Soc. 126 (2004) 52–53.
[8] J. Zhang, L.B. Anna, M. Daniel, Effect of surface pressure on the insulator to metal transition of a langmuir polyaniline monolayer, J. Am. Chem. Soc. 125 (2003) 9312–9313.
[9] M. Rijhwani, L.M. Kanai, Aids for analytical chemists, Anal. Chem. 44 (1972) 2404–2407.
[10] L.H. Wang, J. Sheng, Preparation and properties of polypropylene/org-attapulgite nanocomposites, Polymer 46 (2005) 6243–6249.
[11] Y.S. Liu, P. Liu, Z.X. Su, Core-shell attapulgite@polyaniline composite particles via in situ oxidative polymerization, Synth. Met. 157 (2007) 585–591.
[12] C. Yang, P. Liu, Core-shell attapulgite@polypyrrole composite with well-defined corn cob-like morphology via self-assembling and in situ oxidative polymerization, Synth. Met. 159 (2009) 2056–2062.
[13] J.H. Qiu, H. Feng, Preparation and properties of PAn/ATTP/PE conductive composites, Trans. Nonferr. Met. Soc. 16 (Suppl. 1) (2006) 444–448.
[14] X.P. Lei, Y.S. Liu, Z.X. Su, Synthesis, Characterization of organo-attapulgite/polyaniline-dodecylbenzenesulfonic acid based on emulsion polymerization method, Polym. Composite 29 (2008) 239–244.
[15] W. Jia, E. Segla, D. Kornemandel, Y. Lamhot, M. Narkis, A. Siegmann, Polyaniline-DBSA/organophilic clay nanocomposites: synthesis and characterization, Synth. Met. 128 (2002) 115–120.
[16] D.S. Sutar, N. Padma, D.K. Aswal, S.K. Deshpande, S.K. Gupta, J.V. Yakhmi, Growth of highly oriented crystalline polyaniline films by self-organization, J. Colloid. Interf. Sci. 313 (2007) 353–358.
[17] G.K.R. Senadeera, T. Kitamura, Y. Wada, S. Yanagida, Deposition of polyaniline via molecular self-assembly on TiO_2 and its uses as a sensitiser in solid-state solar cells, J. Photochem. Photobiol. A 164 (2004) 61–66.
[18] L. Jing, Z. Lihua, W. Yinghui, H. Yutaka, Z. Aiqing, T. Heqing, Hybrid composites of conductive polyaniline and nanocrystalline titanium oxide prepared via self-assembling and graft polymerization, Polymer 47 (2006) 7361–7367.
[19] X. Shouhu, J.W. Yixiang, L. Kenchamfai, S. Kangying, Synthesis of Fe_3O_4@polyaniline core/shell microspheres with well-defined blackberry-like morphology, J. Phys. Chem. C 112 (2008) 18804–18809.
[20] Z.F. Li, E. Ruckenstein, Conductive surface via graft polymerization of aniline on a modified glass surface, Synth. Met. 129 (2002) 73–83.
[21] L. Shao, J.H. Qiu, H.X. Feng, M.Z. Liu, G.H. Zhang, J.B. An, et al., Structural investigation of lignosulfonate doped polyaniline, Synth. Met. 159 (2009) 1761–1766.
[22] Z. Jing, K. Lingbin, W. Bin, L. Yongchun, K. Long, In situ electrochemical polymerization of multi-walled carbon nanotube/polyaniline composite films for electrochemical supercapacitors, Synth. Met. 159 (2009) 260–266.
[23] A. Malinauskas, Chemical deposition of conducting polymers, Polymer 42 (2001) 3957–3972.
[24] K.C. Chang, G.W. Jang, C.W. Peng, C.Y. Lin, J.C. Shieh, J.M. Yeh, et al., Comparatively electrochaemical studies at different operational temperatures for the effect of nanoclay plateles on the anticorrosion efficiency of DBSA-doped polyaniline/Na^+-MMT clay nanocomposite coatings, Electrochim. Acta 52 (2007) 5191–5200.
[25] P. Jan, T. Miroslava, H. Drahomira, S. Jaroslav, Conductivity ageing in temperature-cycled polyaniline, Polym. Degrad. Stab. 78 (2002) 393–401.
[26] L.f. Sun, H. Liu, C. Robert, S.C. Yang, Double-Strand Polyaniline, Synth. Met. 84 (1997) 67–68.
[27] E. Vitoratos, S. Sakkopoulos, E. Dalas, P. Malkaj, C. Anestis, D.C. conductivity and thermal aging of conducting zeolite/polyaniline and zeolite/polypyrrole blends, Curr. Appl. Phys. 7 (2007) 578–581.
[28] H.K. Jong, K.S. Hyun, J.K. Hyun, O.Y. Chul, L. Hosull, Structural aspect of metal-insulator transition in doped conducting polymers, Synth. Met. 84 (1997) 71–72.
[29] A. GÖk, M. Omastová, J. ProkeŠ, Synthesis and characterization of red mud/polyaniline composites: Electrical properties and thermal stability, Eur. Polym. J. 43 (2007) 2471–2480.
[30] P. Jan, K. Ivo, T. Eva, J. Stejskal, Enhanced stability of polyaniline/inorganic salt composites during temperature cycling, Polym. Degrad. Stab. 68 (2000) 261–269.
[31] D. Bruno, R. Patrice, F. Pavol, D. David, P.T. Jean, P. Adam, Effect of plasticizing dopants on spectroscopic properties, supramolecular structure, and electrical transport in metallic polyaniline, Chem. Mater. 13 (2001) 4032–4040.
[32] D.H. Droste, A.T. Dibenedetto, The glass transition temperature of filled polymers and its effect on their physical properties, J. Appl. Polym. Sci. 13 (2003) 2149–2168.
[33] N.F. Mott, E.A. Davis, Electronic Procefsses in Noncrystalline Materials, Clarendon, Oxford, 1979.
[34] K. Huang, M.X. Wan, Self-assembled polyaniline nanostructures with photoisomerization function, Chem. Mater. 14 (2002) 3486–3492.
[35] L.J. Zhang, M.X. Wan, Polyaniline/TiO_2 composite nanotubes, J. Phys. Chem. B 107 (2003) 6748–6753.
[36] J.H. Jung, S.H. Hong, J. Joo, Nanocomposite of polyaniline and Na+-montmorillonite clay Bo-Hyun Kim, Macromolecules 35 (2002) 1419–1423.
[37] K.S. Ryu, S.K. Jeong, J. Joo, K.M. Kim, Polyaniline doped with dimethyl sulfate as a nucleophilic dopant and its electrochemical properties as an electrode in a lithium secondary battery and a redox supercapacitor, J. Phys. Chem. B 111 (2007) 731–739.
[38] M. Philipp, M. Martin, B. Armin, D. Wolfgang, Microscopic explanation of the non-Arrhenius conductivity in glassy fast ionic conductors, Phys. Rev. Lett. 77 (1996) 1528–1531.
[39] M. Trchova, I. Sedenkova, E. Tobolkova, J. Stejskal, FTIR spectroscopic and conductivity study of the thermal degradation of polyaniline films, Polym. Degrad. Stab. 86 (2004) 179–185.
[40] S. Quillard, G. Louam, J.P. Buisson, M. Boyer, M. Lapkowski, A. Pron, S. Lefrant, Vibrational spectroscopic studies of the isotope effects in polyaniline, Synth. Met. 84 (1997) 805–806.
[41] J.C. Chiang, A.G. MacDiarmid, 'Polyaniline': Protonic acid doping of the emeraldine form to the metallic regime, Synth. Met. 13 (1986) 193–205.
[42] L. Zhang, T.M. Wang, P. Liu, Polyaniline-coated halloysite nanotubes via in situ chemical polymerization, Appl. Surf. Sci. 255 (2008) 2091–2097.
[43] M.J. Antony, M. Jayakannan, Amphiphilic azobenzenesulfonic acid anionic surfactant for water-soluble, ordered, and luminescent polypyrrole nanospheres, J. Phys. Chem. B 111 (2007) 12772–12780.
[44] P. Rannou, A. Gawlicka, D. Berner, A. Pron, M. Nechtschein, Spectroscpic, Structural and transport properties of conductive polyaniline processed form fluorinated alcohols, Macromolecules 31 (1998) 3007–3015.
[45] L. Shao, J.H. Qiu, M.Z. Liu, H.X. Feng, G.H. Zhang, L.J. Qin, Preparation and characterization of fly ashes and polyaniline core/shell microspheres, Synth. Met. 160 (2010) 143–149.
[46] H. Koshan, H. Tarhwa, K. Chungwen, L. Swuwen, L. Jongjing, H. Yingjie, Effect of aniline formaldehyde resin on the conjugation length and structure of doped polyaniline: spectral studies, J. Polym. Sci. Part A: Pol. Chem. 43 (2005) 3116–3125.
[47] V.Á. Adrián, A.S. José, E.S. Gustavo, Doping of polyaniline by acid–base chemistry: density functional calculations with periodic boundary conditions, J. Am. Chem. Soc. 127 (2005) 11318–11327.
[48] Y.C. Ou, F. Yang, Z.Z. Yu, A new conception on the toughness of nylon 6/silica nanocomposite prepared via in situ polymerization, J. Polym. Sci. Part. B: Polym. Phys. 36 (1998) 789–795.
[49] P. Alexander, O. Nikolay, K. Alexander, S. Galina, Some aspects of preparation methods and properties of polyaniline blends and composites with organic polymers, Prog. Polym. Sci. 28 (2003) 1701–1753.